Current Biology 21, 2092–2097, December 20, 2011 ©2011 Elsevier Ltd All rights reserved DOI 10.1016/j.cub.2011.11.010

Report

Cortactin Releases the Brakes in Actin-Based Motility by Enhancing WASP-VCA Detachment from Arp2/3 Branches

Orit Siton,[1] Yaron Ideses,[1] Shira Albeck,[2] Tamar Unger,[2] Alexander D. Bershadsky,[3,5] Nir S. Gov,[4] and Anne Bernheim-Groswasser[1,*]

[1]Department of Chemical Engineering and Ilse Kats Institute for Nanoscale Science and Technology, Ben-Gurion University of the Negev, Beer-Sheva 84105, Israel

[2]Department of Structural Biology

[3]Department of Molecular Cell Biology

[4]Department of Chemical Physics

Weizmann Institute of Science, Rehovot 76100, Israel

[5]Mechanobiology Institute, National University of Singapore, Singapore 117411

Summary

Cortactin is involved in invadopodia and podosome formation [1], pathogens and endosome motility [2], and persistent lamellipodia protrusion [3, 4]; its overexpression enhances cellular motility and metastatic activity [5–8]. Several mechanisms have been proposed to explain cortactin's role in Arp2/3-driven actin polymerization [9, 10], yet its direct role in cell movement remains unclear. We use a biomimetic system to study the mechanism of cortactin-mediated regulation of actin-driven motility [11]. We tested the role of different cortactin variants that interact with Arp2/3 complex and actin filaments distinctively. We show that wild-type cortactin significantly enhances the bead velocity at low concentrations. Single filament experiments show that cortactin has no significant effect on actin polymerization and branch stability, whereas it strongly affects the branching rate driven by Wiskott-Aldrich syndrome protein (WASP)-VCA fragment and Arp2/3 complex. These results lead us to propose that cortactin plays a critical role in translating actin polymerization at a bead surface into motion, by releasing WASP-VCA from the new branching site. This enhanced release has two major effects: it increases the turnover rate of branching per WASP molecule, and it decreases the friction-like force caused by the binding of the moving surface with respect to the growing actin network.

Results and Discussion

The polymerization of actin is directed to the surface of the cell membrane or vesicles, by localizing to the surface Wiskott-Aldrich syndrome protein (WASP), which then activates the branching of the filaments using the Arp2/3 complex. The actin network that forms at the surface produces an elastic pushing force on the surface. However, the same WASP molecule that initiates actin polymerization also inherently inhibits the translation of the protrusive force into motion, by binding to the same actin network. This is an inherent problem, because in order to localize the branching process to the membrane, the WASP molecule has to make contact with the network during the formation of the new branch. We find that cortactin plays a critical role in enhancing the ability to translate actin polymerization at a surface into motion, by releasing WASP molecules from the new branching site.

We investigated how cortactin affects the velocity of VCA-coated beads. Addition of wild-type (WT) GST-cortactin affected the beads' velocity $v(c)$ nonmonotonously. In Figure 1A we show the normalized velocity $v(c)/v(0)$ versus cortactin concentration c. Below 800 nM cortactin enhanced the bead velocity, whereas above it, the velocity decayed as $c^{-\nu}$ with $\nu = 1.34 \pm 0.01$ (inset, Figure 1A). Replacing VCA with WT cortactin did not produce any movement; the beads only polymerized a thin actin layer around their surface, which never evolved into a comet tail (see Figures S1A–S1D available online).

In order to determine whether changes in the density of the actin gel $\rho_{bead}(c)$ were responsible for the observed changes in the beads' velocity, we measured the gray-level intensity of the actin network behind the bead (Supplemental Experimental Procedures). The normalized density of the actin gel, $\rho_{bead}(c)/\rho_{bead}(0)$, versus c is depicted in Figure 1A. In contrast to the velocity, the density of the actin gel barely changes up to 1,200 nM cortactin. Above 1,200 nM we observe a decay of $\rho_{bead}(c)/\rho_{bead}(0)$ with c.

We used fluorescence recovery after photobleaching (FRAP) to study the dynamics of cortactin and actin in the vicinity of the beads and along the comet. Although cortactin distributes in proportion to the actin density (Figure 1B), their dynamics are distinct (Figures S1E and S1F; Supplemental Experimental Procedures): cortactin rapidly exchange throughout the entire comet, whereas actin follows a treadmilling behavior, in accord with in vivo results [12].

The possible effects of cortactin that modify the beads velocity can arise from either a change in the effective protrusive force produced by the actin network and/or by reducing the effective friction arising from the transient binding of the actin network to the bead surface (via VCA molecules) [13–15]. The effect on the protrusive forces can be either through modification of the density of polymerizing barbed ends near the surface, changes in filaments' elongation rates, and/or by affecting the force per filament. In the later case, cortactin could possibly affect the stiffness of the actin filaments and this could affect the force produced per filament [16].

We used total internal reflection fluorescence (TIRF) microscopy to investigate the effect of cortactin on filament elongation and branching rates. The experimental system consisted of actin, Arp2/3 complex, VCA, and increasing amounts of WT cortactin (0–8,000 nM) (Figure S2A; Movie S1; Movie S2; Movie S3). The protocol for this assay follows Kuhn and Pollard [17]. For each cortactin concentration, we analyzed the elongation rate $v_p(c)$ of a set of 15 filaments (Figure S2B). Using the distribution of measured elongation rates (Figure S2C), we calculated the mean value (Figure 2A). Up to 2,000 nM cortactin, the normalized elongation rate is practically independent of c, in agreement with previous bulk measurements [18], and has a mean value of $v_p(c)/v_p(0) = 0.94 \pm 0.13$, where $v_p(0) = 9.5 \pm 0.57$ *sub*/sec. Only for larger concentrations, $c \geq$ 4,000 nM, we observed a decay of $v_p(c)/v_p(0)$ with c (inset, Figure 2A). At high concentrations ($c \geq$ 4,000 nM), we also observed a reduction in the proportion of filaments that

*Correspondence: bernheim@bgu.ac.il

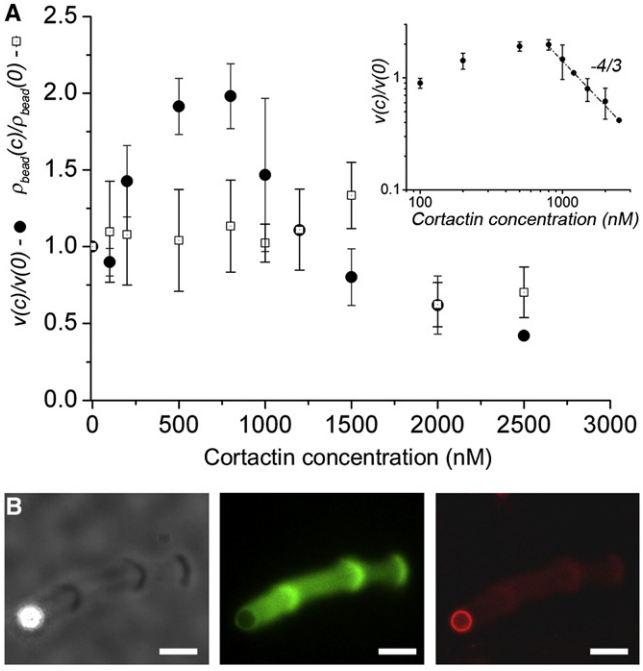

Figure 1. Cortactin Effect on the Bead Velocity and Gel Density

(A) Normalized velocity of the bead (black circles) and density of the actin gel (black hollow squares) as a function of the cortactin concentration. The inset shows the normalized velocity in a log-log scale. At high concentrations, the velocity decays as $c^{-4/3}$. Values correspond to mean ± SD.

(B) Colocalization of actin and cortactin along the comet tail. Bead diameter d = 4.78 μm. The motility medium consists of 7 μM F-actin, 1.0 μM GST-cortactin, 0.7 μM G-actin, and 142 nM GST-cortactin labeled with Alexa Fluor 488 and 568, respectively. Left to right: phase contrast and fluorescence images of actin and cortactin, respectively. The data shows that cortactin (red) distributes over the entire actin (green) network in proportion to the actin density. Scale bars represent 10 μm.

attached firmly to the surface (Figure S3A; Movie S3; and Supplemental Experimental Procedures). The reduced affinity to the N-ethylmaleimide (NEM)-myosin molecules infer on a possible adsorption (decoration) of cortactin along the filaments' backbone, thus blocking available attachment sites.

Next, we investigated how cortactin mediated the formation of actin branches by VCA and Arp2/3 complex. The effect of WT cortactin on filament branching is nonmonotonic; at low c, cortactin enhances the nucleation of branches, whereas at high c it inhibits their formation (Figure 2B). Plotting the normalized branching rate (per unit length) K_{branch} (Supplemental Experimental Procedures) versus c revealed an initial linear growth up to ~50 nM (Figure 2B, upper inset), followed by an abrupt decay of K_{branch} as $1/c$ (Figure S3B, inset b). We repeated the experiments at a higher frame rate (1 s instead of 10 s between frames) and found that the branches were completely stable, irrespective of cortactin [18]. Under these conditions, we therefore purely measure cortactin's effect on the branching rate.

Our observations, together with published data, lead us to propose that the dominant processes involving cortactin in this system are as follows: (1) VCA is the main branch nucleator and is dominant over cortactin-induced branching, (2) cortactin has an affinity to VCA/Arp2/3 complex/F-actin and tends to enhance the dissociation rate of VCA from such complexes [10, 19], and (3) cortactin has an affinity to F-actin [20, 21] and tends to decorate its backbone. These observations suggest that WT cortactin can increase the branching rate by releasing VCA from bound Arp2/3 complexes and increasing its overall activity. On the other hand, at large concentrations, cortactin decorates the actin filaments and inhibits VCA/Arp2/3 complex from attaching to the filaments and initiating a new branch (depletion of Arp2/3 complex from the branching cycle by binding to cortactin in solution is an alternative process but was shown to be 20-fold less effective compared to the binding of cortactin to bare F-actin [20, 21]). These opposing processes may lead to the observed nonmonotonic behavior of the bead velocity and branching rate (Figure 1; Figure 2).

In order to explore the validity of these conclusions, we repeated the experiments using two cortactin variants; a NTA fragment lacking the F-actin binding domain, and a mutant lacking the acidic DDW motif that binds the Arp2/3 complex. The effect of these variants on the branching rate is shown in the lower inset of Figure 2B. We find that the NTA fragment is effective in increasing the branching rate, although less than WT cortactin, whereas the DDW mutant only interferes with the branching process.

In Figure 3A we plot the velocity of the bead for the different cortactin variants. We find that the velocity is monotonously increasing with NTA concentration, as expected if this fragment cannot attach (decorate) F-actin. For the DDW mutant, we find that it is unable to increase the bead motility. In Figure 3B we plot the reduced actin gel densities behind the bead for the three cortactin variants. Compared to the WT, we find that both variants induce a gel of lower density.

In order to study the mechanism by which cortactin functions in actin-based movement, we estimated the net branching rate per unit length behind the moving bead, $K_{branch,\ b}$, by multiplying the measured bead velocity and gel density (see Text 2, Supplemental Information). For WT cortactin we find that $K_{branch,\ b}$ behaves (qualitatively) similarly (inset of Figure 3B) to K_{branch} measured on individual (static) filaments (Figure 2B). Increase in the net branching rate at low c could result from stabilization of the newly-formed branches by cortactin (i.e., preventing debranching), yet the fact that cortactin rapidly exchange through the comet (Figures S1E and S1F) infer on a weak binding energy associated with the formation of an Arp2/3/F-actin/cortactin complex. Taken together, these experimental findings strongly support our proposed mechanism by which the dominant role of cortactin in enhancing Arp2/3-based actin motility is to release the VCA from the Arp2/3-F-actin complex and not to stabilize the newly-formed branches. Finally, the lack of decay in the branching activity (Figure 3B, inset) and motility (Figure 3A) for the NTA fragment indicates that the observed decay for the WT and DDW mutant is related to their ability to bind and decorate bare F-actin.

From our proposed mechanism of cortactin activity in Arp2/3 branching, we write a model of steady-state chemical reactions (Figure S3A, Text 1 in Supplemental Information). This model allows us to calculate the dependence of the measured branching rate per unit length $K_{branch}(c)$ on WT cortactin concentration (equation S8, Figure S3B). The same formula can be used to fit the dependence of the density of the actin gel behind the bead, $\rho_{bead}(c)$

$$\rho_{bead}(c) = \frac{Ac + B}{Dc^2 + Ec + G} \qquad \text{(Equation 1)}$$

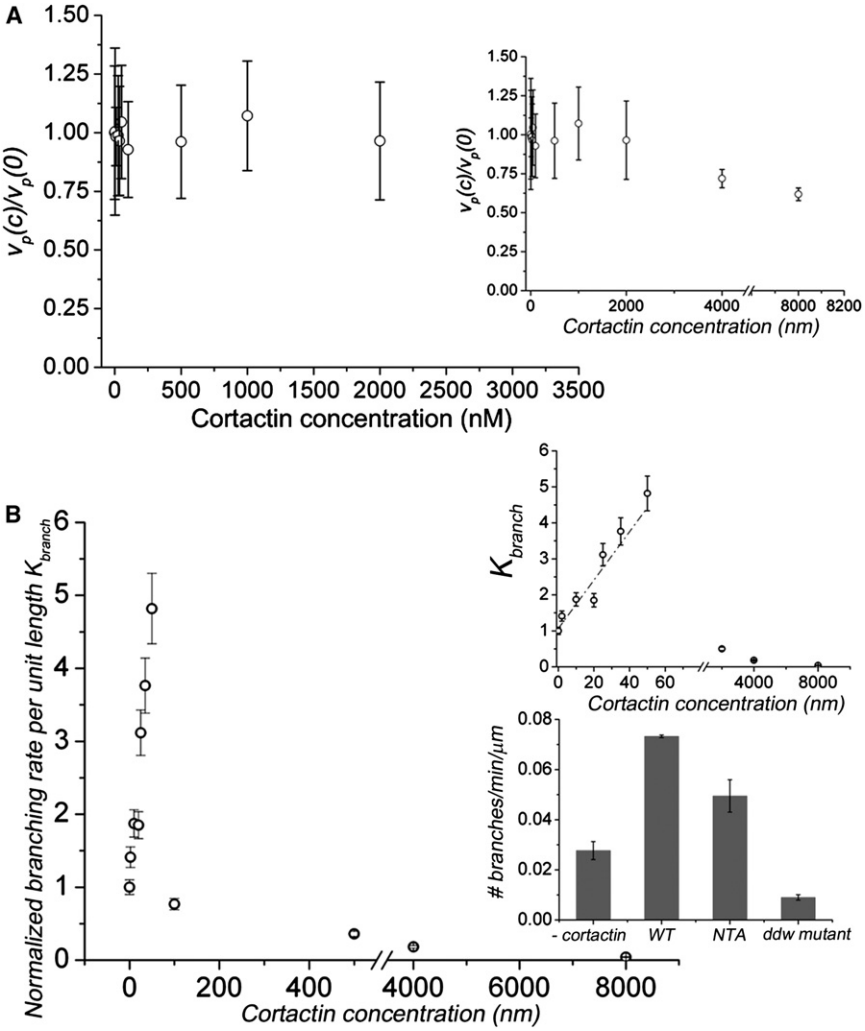

Figure 2. Polymerization and Branching Rates of Individual Actin Filaments

(A) Normalized elongation rate of actin filaments as a function of cortactin concentration (0–2,000 nM). Inset shows normalized elongation rate as a function of cortactin concentration *c* ranging between 0 and 8,000 nM. Up to 2,000 nM cortactin, the elongation rate is approximately constant. Above this concentration, the elongation rate decreases with *c*. Values correspond to mean ± SD.

(B) Normalized branching rate (per unit length) K_{branch} as a function of cortactin concentration *c*. The low cortactin concentration region is characterized by a linear increase in the branching rate (upper-inset: the dash-dot line was determined by linear regression), whereas above ~50–100 nM, the branching rate decays with cortactin concentration. In the lower inset, the branching rate (per unit length) for three different cortactin variants is depicted: wild-type (WT), NTA fragment (NTA), and DDW mutant (DDW), and in the absence of cortactin (−cortactin). Values correspond to mean ± SD.

In Figure 3B we plot the measured (normalized) gel density for WT cortactin with the fit where the fitting parameters are given in Figure S3D. We see that at large *c*, $\rho_{bead}(c) \sim c^{-1}$.

We now describe the effect of cortactin on the bead velocity. In overdamped dynamics, the bead velocity is given by

$$v(c) = \frac{F(c)}{\gamma(c)} \qquad \text{(Equation 2)}$$

where $F(c) \propto K_{gel}(c)\,\rho_{VCA}$ is the cortactin-dependent pushing force per unit area [$K_{gel}(c)$ is the gel elastic modulus, and ρ_{VCA} is the areal concentration of actin nucleators (VCA)] and $\gamma(c)$ is the cortactin-dependent effective friction coefficient per unit area (Text 2 in Supplemental Information). In [13, 14] it was shown that $K_{gel}(c) \propto \rho_{bead}(c)^{4/3}$. Thus for a constant friction coefficient γ in Equation 2, $v(c) \propto \rho_{bead}(c)^{4/3}$. This relation describes perfectly the bead velocity for the DDW mutant (Figure 3A), as expected, because DDW does not interfere with the VCA/Arp2/3 complex binding and therefore does not modify the effective friction coefficient. This relation also fits the velocity of WT cortactin for c > 1,000 nM (solid line, Figure 3A). Using the fit for $\rho_{bead}(c)$ (Equation 1) to the power of 4/3, we recover the measured dependence of $v(c) \propto c^{-4/3}$ at large *c* (Figure 1A).

However, for small WT cortactin concentrations, the bead velocity raises much faster compared to the very slight increase in the gel density (Figure 1A). We can fit this part of the data very well, by including the cortactin-induced reduction in the effective friction coefficient $\gamma(c)$ (Equation S9, Supplemental Information) with the fitting parameters given in Figure S3E. From this fit we find that WT cortactin reduces the bead and the actin network by 25%. As seen in Figure 3A, we could not fit the whole data range using a single expression for the dependence of the effective friction coefficient on *c*. Note that the expressions we are using for the dependence of both $\rho_{bead}(c)$ and $\gamma(c)$ on *c* are based on steady-state chemical reactions and do not treat explicitly the effects of the velocity of the moving bead on these quantities. A full dynamical simulation is needed for a more realistic calculation [22, 23].

Using similar scaling arguments, we can explain the observed behavior for the velocity in the case of the NTA fragment. In Figure 3B inset we see that the branching rate for NTA is almost unchanged and roughly constant, i.e., $K_{branch,\,b} \cong 1$. Therefore, the velocity is only modified by the reduction in the effective friction coefficient (Text 2 in Supplemental Information). Using the same model and fitting parameters for $\gamma(c)$ as for WT cortactin (Figure S3E), we find an excellent agreement to the NTA fragment velocity data (Figure 3A).

In this work we combine direct imaging of individual filament branching and bead motility assay to study the mechanism of cortactin-mediating actin-based movement. Overall, our data suggest that in contrast to the prevailing hypotheses that cortactin stabilizes Arp2/3-mediated branched filament junctions [18], the increase in the branching rate is associated with cortactin's capability to enhance the release of VCA from the VCA/Arp2/3 complex/F-actin complexes, thereby allowing it to have a higher turnover rate (Figure 4). We find that WT cortactin is able to efficiently release VCA and increase the branching

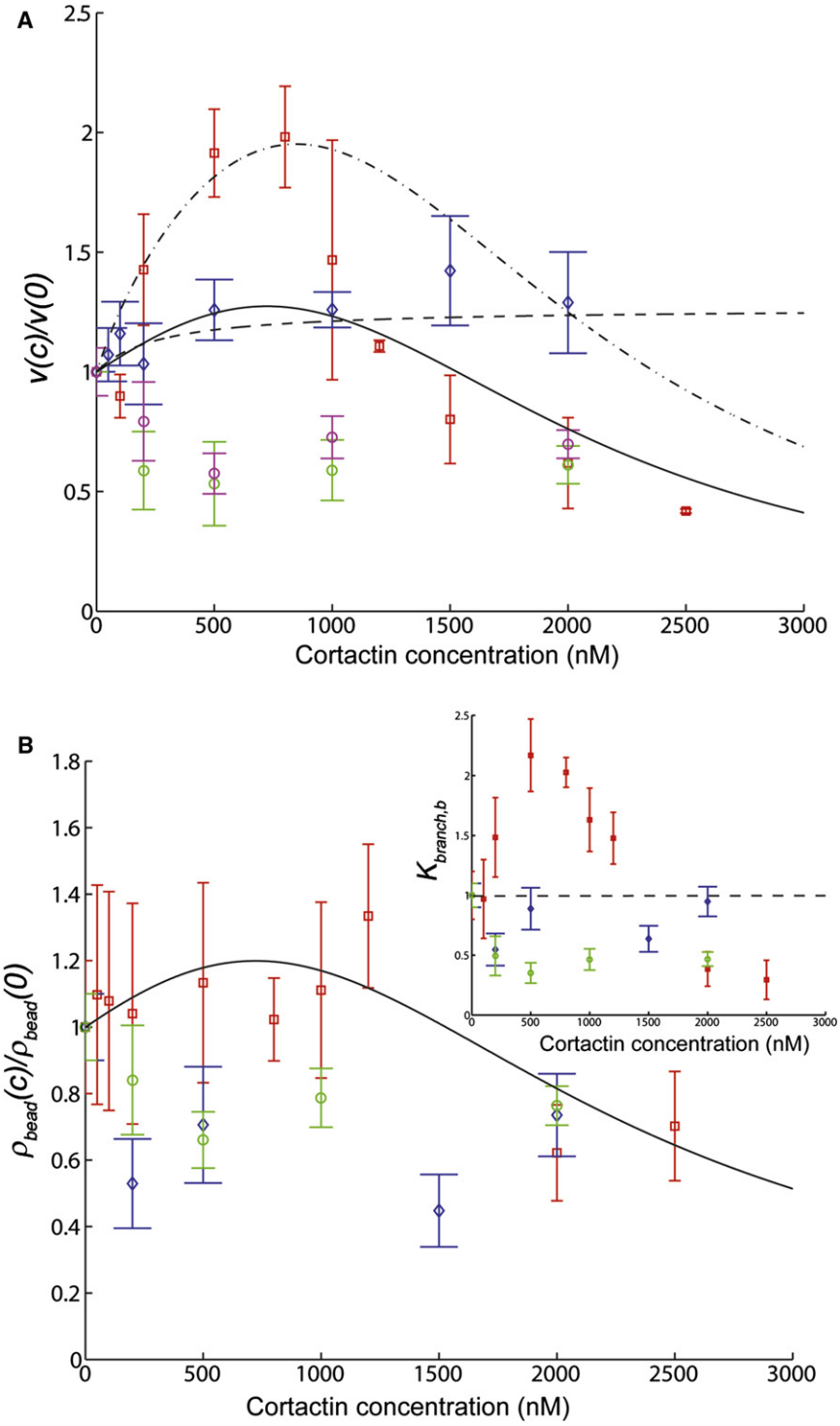

Figure 3. Data Analysis and Modeling

(A) Normalized velocity of the bead as a function of cortactin concentration for the three cortactin variants. Experimental data are as follows: WT cortactin, red squares; NTA fragment, blue diamonds; and DDW mutant, green circles. Values correspond to mean ± SD. The model calculations using Equation 2 are given by the lines; for the WT cortactin, the dashed-dot line is calculated using the cortactin-dependent effective friction (Equation S9, Supplemental Information), whereas the solid line for a constant friction such that $v(c) \propto \rho_{bead}(c)^{4/3}$ (in this equation, we use the fit for the gel density [see B below] using the functional form given in Equation 1). For the DDW mutant, the magenta circles are the prediction for the velocity based on the data of the gel density (green circles in B) to the power of 4/3. The NTA velocity curve is fitted by $v(c) \propto 1/\gamma(c)^{3/7}$ (dashed line) given NTA-dependent effective friction (Equations S9–S11 in Supplemental Information).

(B) Normalized density of the actin gel near the bead surface as a function of the cortactin concentration for the three cortactin variants: WT, red squares; NTA fragment, blue diamonds; and DDW mutant, green circles. The solid line gives the fit for the WT cortactin data using the functional form given in Equation 1. Inset shows the normalized branching rate behind the bead $K_{branch,b}$ for the three cortactin variants (symbols as in B). The dashed line in the inset denotes the value $K_{branch,b}(c) \sim 1$ to show that the NTA is to a good approximation behaving like this (details are given in Text 2 in Supplemental Information). Values correspond to mean ± SD.

rate near the moving bead, whereas the NTA fragment is not (Figure 3B, inset). We conclude that the WT's affinity to F-actin enhances its efficacy, compared to NTA, in releasing the VCA from the newly-formed junction. This added efficiency at low concentrations has the price of an inhibitory effect at large concentration, due to the same affinity to F-actin (Figure 4). Our results are also in accord with biochemical studies postulating that cortactin is regulating the reduced affinity of WASP for the Arp2/3 complex [10], after actin nucleation is initiated, which is required for rapid motility [24].

How does this mechanism of action explain cortactin's function in vivo? Cortactin is involved in cellular migration, trafficking processes, and pathogens propulsion. Overexpression of cortactin enhances lamellipodial persistence and cell motility, whereas its depletion leads to instable and rapidly retracting protrusions [3, 4]. The effect of cortactin on endosome [25, 26] and pathogen motility was not directly tested. Yet, the importance of detachment of newly formed actin branches from the moving surface is demonstrated by the observation that whereas WT *Listeria* propels rapidly and persistently, mutated *Listeria* with impaired detachment resulted in an irregular slow motion [27]. This demonstrates that the cortactin-induced release mechanism can explain cortactin's observed role in cellular propulsion.

Experimental Procedures

Preparation of VCA and Cortactin-Coated Beads

Polystyrene Beads (Polysciences) were incubated in solutions of 5 μM GST-VCA or GST-cortactin variants for 30 min. The surface of the beads was further passivated with a solution of 10% bovine serum albumin

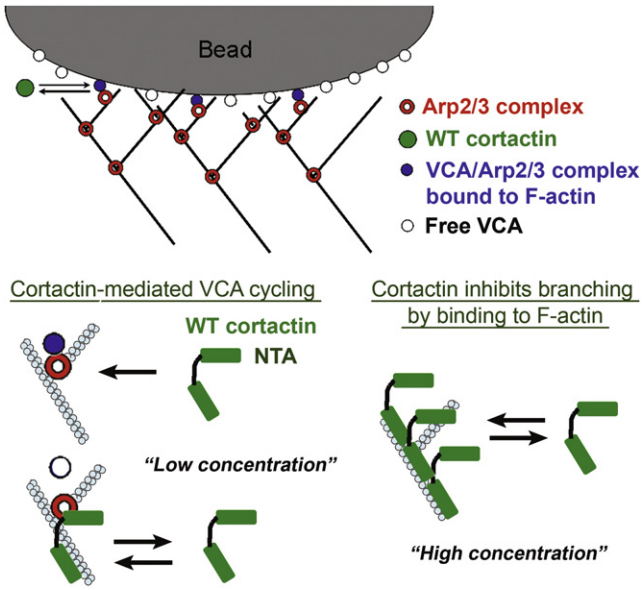

Figure 4. Mechanism of Cortactin's Function in Actin-Driven Polymerization

Schematic diagram showing a bead coated with VCA molecules polymerizing a branch actin network at its surface through the activation of Arp2/3 complex. At low concentrations, cortactin enhance the release of VCA molecules from the newly-formed branches, whereas at high concentrations, it has an inhibitory effect due to its high affinity to F-actin.

(BSA) according to the protocol detailed in [11]. All beads were used within 24 hr.

Beads Motility Assay

The motility medium contained 10 mM HEPES (pH 7.6), 1.7 mM Mg-ATP, 5.5 mM DTT, 0.12 mM 1,4 diazabicyclo[2.2.2]octane (Dabco), 0.05 MKCl, 2 mM MgCl2, 7 μM F-actin, 0.1 μM Arp2/3 complex, 0.04 μM capping protein, 3.5 μM cofilin, 3 μM profilin, 0.7 μM G-actin labeled with Alexa Fluor 568, 0.75% BSA, and various concentrations (0–2,500 nM) of GST-cortactin variants (WT, NTA fragment [residues 1–84], or DDW mutant [in-frame deletion of residues (20–22) from the NTA domain]). The movement of the microspheres with respect to the comet tail was followed for ~1–1.5 hr. In all the (bead motility) experiments, we used GST-cortactin. Similar results were obtained with cleaved cortactin (lacking GST), suggesting that dimerization is not playing an essential role in cortactin function. Measurements of the beads' velocity and the gel density ρ_{bead} along the comets (see details in Supplemental Information) were done using METAMORPH (Molecular Devices). Measurements were performed on about 10 beads for each concentration of cortactin used. Fitting of the experimental data was performed using Matlab (MathWorks) and Origin (Originlab).

Single Actin Filament TIRF Assays

The protocol for this assay was kindly provided by Jeff Kuhn [17]. We followed the growth and branching of individual filaments until overlapping between filaments was observed. Samples were excited by total internal reflection illumination at 488 nm, and images were captured with an Andor backilluminated DU-897 EMCCD camera controlled by Leica software (LAS-AF-6000, 2.2.0 build 4758, Leica Microsystems CMS GmbH, Germany) on a Leica DMI6000 B.

Supplemental Information

Supplemental Information Includes three figures, Supplemental Data, Supplemental Experimental Procedures, and three movies and can be found with this article online at doi:10.1016/j.cub.2011.11.010.

Acknowledgments

A.D.B. is grateful to A.M. Weaver for kindly providing the WT cortactin construct and to S. Weed for the constructs of the NTA fragment and DDW mutant. A.B.-G. is grateful to P. Lappalainen for kindly providing mouse capping protein construct, to H. Higgs for his kind gift of the profilin construct, and to L. Blanchoin for the cofilin construct. We thank Yellena Mirsky with the help with FRAP experiments. We would like to thank Alexander Mogilner, Gilad Haran, and David Gillo for careful reading of the manuscript and useful comments. A.B.-G. thanks the Israel Cancer Association (grant no. 20070020B) and the Israel Science Foundation (grants no. 551/04 and 1534/10) for financial support. A.D.B. holds the Joseph Moss Professorial Chair in Biomedical Research and acknowledges support from the Israel Science Foundation, Minerva Foundation, and Maurice Janin Fund. N.S.G. thanks the Alvin and Gertrude Levine Career Development Chair and the Binational Science Foundation grant no. 2006285 for their support.

Received: May 27, 2011
Revised: September 29, 2011
Accepted: November 4, 2011
Published online: December 8, 2011

Reference List

1. Luxenburg, C., Geblinger, D., Klein, E., Anderson, K., Hanein, D., Geiger, B., and Addadi, L. (2007). The architecture of the adhesive apparatus of cultured osteoclasts: from podosome formation to sealing zone assembly. PLoS ONE *2*, e179.
2. Zettl, M., and Way, M. (2001). New tricks for an old dog? Nat. Cell Biol. *3*, E74–E75.
3. Bryce, N.S., Clark, E.S., Leysath, J.L., Currie, J.D., Webb, D.J., and Weaver, A.M. (2005). Cortactin promotes cell motility by enhancing lamellipodial persistence. Curr. Biol. *15*, 1276–1285.
4. Boguslavsky, S., Grosheva, I., Landau, E., Shtutman, M., Cohen, M., Arnold, K., Feinstein, E., Geiger, B., and Bershadsky, A. (2007). p120 catenin regulates lamellipodial dynamics and cell adhesion in cooperation with cortactin. Proc. Natl. Acad. Sci. USA *104*, 10882–10887.
5. Daly, R.J. (2004). Cortactin signalling and dynamic actin networks. Biochem. J. *382*, 13–25.
6. Yamaguchi, H., and Condeelis, J. (2007). Regulation of the actin cytoskeleton in cancer cell migration and invasion. Biochim. Biophys. Acta *1773*, 642–652.
7. Weaver, A.M. (2008). Cortactin in tumor invasiveness. Cancer Lett. *265*, 157–166.
8. Desmarais, V., Yamaguchi, H., Oser, M., Soon, L., Mouneimne, G., Sarmiento, C., Eddy, R., and Condeelis, J. (2009). N-WASP and cortactin are involved in invadopodium-dependent chemotaxis to EGF in breast tumor cells. Cell Motil. Cytoskeleton *66*, 303–316.
9. Weaver, A.M., Heuser, J.E., Karginov, A.V., Lee, W.L., Parsons, J.T., and Cooper, J.A. (2002). Interaction of cortactin and N-WASp with Arp2/3 complex. Curr. Biol. *12*, 1270–1278.
10. Uruno, T., Liu, J., Li, Y., Smith, N., and Zhan, X. (2003). Sequential interaction of actin-related proteins 2 and 3 (Arp2/3) complex with neural Wiscott-Aldrich syndrome protein (N-WASP) and cortactin during branched actin filament network formation. J. Biol. Chem. *278*, 26086–26093.
11. Bernheim-Groswasser, A., Wiesner, S., Golsteyn, R.M., Carlier, M.F., and Sykes, C. (2002). The dynamics of actin-based motility depend on surface parameters. Nature *417*, 308–311.
12. Lai, F.P., Szczodrak, M., Block, J., Faix, J., Breitsprecher, D., Mannherz, H.G., Stradal, T.E., Dunn, G.A., Small, J.V., and Rottner, K. (2008). Arp2/3 complex interactions and actin network turnover in lamellipodia. EMBO J. *27*, 982–992.
13. Gerbal, F., Noireaux, V., Sykes, C., Julicher, F., Chaikin, P., Ott, A., Prost, J., Golsteyn, R.M., Friederich, E., Louvard, D., et al. (1999). On the 'listeria' propulsion mechanism. Pramana *1*, 155–170.
14. Gerbal, F., Chaikin, P., Rabin, Y., and Prost, J. (2000). An elastic analysis of Listeria monocytogenes propulsion. Biophys. J. *79*, 2259–2275.
15. Bernheim-Groswasser, A., Prost, J., and Sykes, C. (2005). Mechanism of actin-based motility: a dynamic state diagram. Biophys. J. *89*, 1411–1419.
16. Mogilner, A., and Oster, G. (1996). Cell motility driven by actin polymerization. Biophys. J. *71*, 3030–3045.
17. Kuhn, J.R., and Pollard, T.D. (2005). Real-time measurements of actin filament polymerization by total internal reflection fluorescence microscopy. Biophys. J. *88*, 1387–1402.
18. Weaver, A.M., Karginov, A.V., Kinley, A.W., Weed, S.A., Li, Y., Parsons, J.T., and Cooper, J.A. (2001). Cortactin promotes and stabilizes Arp2/3-induced actin filament network formation. Curr. Biol. *11*, 370–374.

19. Soderling, S.H. (2009). Grab your partner with both hands: cytoskeletal remodeling by Arp2/3 signaling. Sci. Signal. *2*, pe5.
20. Uruno, T., Liu, J., Zhang, P., Fan Yx, Egile, C., Li, R., Mueller, S.C., and Zhan, X. (2001). Activation of Arp2/3 complex-mediated actin polymerization by cortactin. Nat. Cell Biol. *3*, 259–266.
21. Pant, K., Chereau, D., Hatch, V., Dominguez, R., and Lehman, W. (2006). Cortactin binding to F-actin revealed by electron microscopy and 3D reconstruction. J. Mol. Biol. *359*, 840–847.
22. Lee, K.C., and Liu, A.J. (2008). New proposed mechanism of actin-polymerizationdriven motility. Biophys. J. *10*, 4529–4539.
23. Carlsson, A.E. (2001). Growth of branched actin networks against obstacles. Biophys. J. *81*, 1907–1923.
24. Dayel, M.J., Holleran, E.A., and Mullins, R.D. (2001). Arp2/3 complex requires hydrolyzable ATP for nucleation of new actin filaments. Proc. Natl. Acad. Sci. *98*, 14871–14876.
25. Kaksonen, M., Peng, H.B., and Rauvala, H. (2000). Association of cortactin with dynamic actin in lamellipodia and on endosomal vesicles. J. Cell. Sci. *113*, 4421–4426.
26. Ohashi, E., Tanabe, K., Henmi, Y., Mesaki, K., Kobayashi, Y., and Takei, K. (2011). Receptor sorting within endosomal trafficking pathway is facilitated by dynamic actin filaments. PLoS ONE *6*, e19942.
27. Lasa, I., Gouin, E., Goethals, M., Vancompernolle, K., David, V., Vandekerckhove, J., and Cossart, P. (1997). Identification of two regions in the N-terminal domain of ActA involved in the actin comet tail formation by Listeria monocytogenes. EMBO J. *16*, 1531–1540.